

BITLIS EREN ÜNIVERSITESI FEN BILIMLERI DERGISI



ISSN: 2147-3129 / e-ISSN: 2147-3188

Article Type: Research Article
Received: June 8, 2025
Revised: July 21, 2025
Accepted: July 30, 2025

DOI : 10.17798/bitlisfen.1715597

Year : 2025 Volume : 14 Issue : 3

Pages : 1787-1801



TOWARD A SAFER AND GREENER FUTURE: RELIABLE AQUEOUS AMMONIUM-ION BATTERIES WITH LiMnO₂ CATHODES

Dilara OZGENÇ ¹ , Melisa UÇAN ¹ , Burak TEKİN ^{1,*}

¹ Ondokuz Mayıs University, Chemical Engineering Department, Samsun, Türkiye * Corresponding Author: burak.tekin@omu.edu.tr

ABSTRACT

Ammonium-ion-based energy storage systems have gained attention as a sustainable alternative for efficient charge storage. In this study, LiMnO₂ is explored for the first time as a cathode material in an aqueous ammonium-ion battery using a 2M (NH₄)₂SO₄ electrolyte. XRD analysis confirms the formation of phase-pure, highly crystalline orthorhombic LiMnO₂, while SEM imaging reveals a nanorod morphology that enhances ion transport. Cyclic voltammetry identifies two distinct charge storage mechanisms: NH4+ insertion/extraction and surfacecontrolled redox reactions, with oxidation peaks at 0.89 V and 0.72 V vs. Ag/AgCl and reduction peaks at 0.53 V and 0.28 V vs. Ag/AgCl. Galvanostatic charge-discharge testing demonstrates an initial discharge capacity of ~60 mAh/g at 1C, stabilizing at ~50 mAh/g after the second cycle and maintaining excellent capacity retention over 130 cycles. The stable electrochemical performance suggests that LiMnO2 undergoes minimal structural degradation, while the mildly acidic (NH₄)₂SO₄ electrolyte effectively mitigates Mn dissolution. Electrochemical impedance spectroscopy reveals a moderate increase in charge transfer resistance (Rct) from 135 Ω to ~200 Ω after cycling, indicating stable interfacial kinetics. The successful demonstration of LiMnO₂ as a hosting material in an aqueous ammonium-ion battery highlights its potential for nextgeneration energy storage applications.

Keywords: Aqueous ammonium ion batteries, Lithium manganese oxide, Ammonium-ion

intercalation, Electrochemical performance, Energy storage materials.

1 INTRODUCTION

With the increasing global demand for sustainable and high-performance energy storage solutions, researchers have explored a wide range of battery technologies beyond conventional lithium-ion systems [1]. Among these emerging alternatives, aqueous ammonium-ion batteries (AAIBs) have garnered significant attention due to their potential advantages in terms of safety, cost-effectiveness, and environmental sustainability. Unlike lithium-ion batteries, which rely on expensive and sometimes geopolitically constrained metal resources such as lithium and cobalt, AAIBs make use of abundant ammonium ions (NH₄⁺) as charge carriers [2]. The utilization of an aqueous electrolyte further enhances their appeal by offering intrinsic non-flammability, higher ionic conductivity, and simplified battery assembly compared to non-aqueous counterparts [3-6]. Furthermore, AAIBs operate under mild pH conditions, which reduces corrosion-related degradation and extends battery lifespan. Given these advantages, AAIBs represent a promising candidate for next-generation, sustainable energy storage applications [7, 8].

The fundamental working principle of aqueous ammonium-ion batteries revolves around the reversible insertion and extraction of NH₄⁺ ions in suitable electrode materials [9]. The unique properties of the NH₄⁺ ion, including its small size, high mobility, and hydrogenbonding capability, play a crucial role in the electrochemical behavior of the battery (Figure 1) [10]. However, these properties also introduce certain challenges, such as the stability of the NH₄⁺ intercalation process and the structural integrity of electrode materials during prolonged cycling [7]. To address these concerns, researchers have explored various cathode and anode materials, including transition metal oxides [10], Prussian blue analogies [11], and Organic polymer materials [12], which exhibit compatibility with NH₄⁺ ion insertion and extraction. Additionally, hybrid nanostructured electrodes have been proposed to enhance ion diffusion kinetics and improve overall electrochemical performance. The choice of electrolyte composition is another critical aspect influencing the performance of AAIBs, as factors such as pH, ionic strength, and solubility limits can significantly affect battery efficiency and longevity [13].

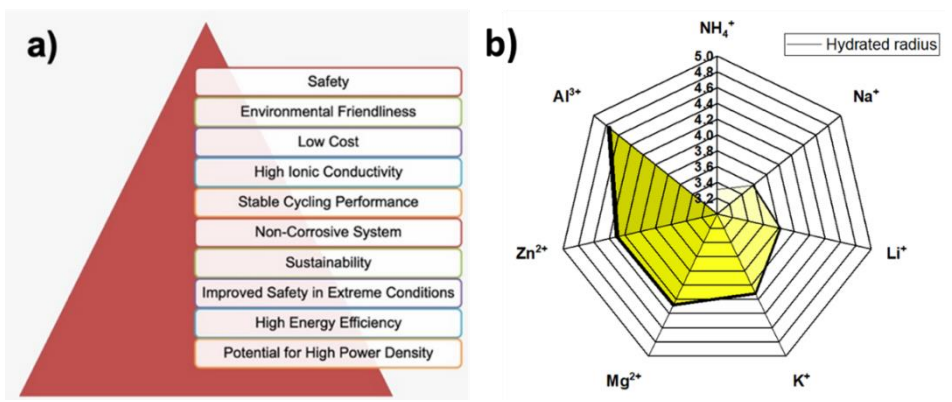


Figure 1. a) Advantages of aqueous ammonium-ion batteries and b) Comparison of atomic radii of different cation carriers.

In recent years, advancements in materials science and electrochemical engineering have led to substantial progress in the development of AAIBs. Novel electrode materials with enhanced electrochemical stability and optimized structural frameworks have been designed to accommodate the unique characteristics of NH₄⁺ ions. Additionally, innovations in electrolyte formulation, including the incorporation of stabilizing additives and buffering agents, have contributed to improved cycle life and energy density [14]. Despite these advancements, several challenges remain, particularly in achieving higher voltage windows, minimizing side reactions, and mitigating capacity fading over extended cycling. In-depth studies on electrode-electrolyte interfaces have revealed that solvation effects and hydrogen bonding interactions significantly influence the mobility and reversibility of NH₄⁺ ions. Addressing these challenges requires a comprehensive understanding of the fundamental ion transport mechanisms, electrode-electrolyte interactions, and the role of solvation effects in AAIBs [15].

The potential applications of aqueous ammonium-ion batteries span a broad range of energy storage needs, including grid-scale energy storage, backup power systems, and portable electronics. Their inherent advantages, such as low toxicity and ease of disposal, align well with the growing emphasis on green energy solutions. Furthermore, the compatibility of AAIBs with renewable energy sources, such as solar and wind power, highlights their potential role in facilitating a more sustainable and resilient energy infrastructure. Ongoing research in operando characterization techniques, such as in-situ spectroscopy and electrochemical impedance spectroscopy, has provided deeper insights into the dynamic behavior of NH₄⁺ ions during charge-discharge cycles, aiding in the rational design of next-generation AAIBs [16-18]. Future research efforts should focus on overcoming existing technical limitations through advanced material design, in-depth mechanistic studies, and system-level optimization. By addressing these aspects, AAIBs could emerge as a viable and scalable energy storage solution,

complementing or even surpassing existing battery technologies in specific applications. The continued exploration of aqueous ammonium-ion batteries is not only of scientific interest but also holds the promise of contributing to a cleaner and more sustainable energy landscape [19].

In this study, we synthesized LiMnO₂ cathode material via a solid-state method and characterized its structural and electrochemical properties for ammonium-ion battery applications. The synthesized material was analyzed using X-ray diffraction (XRD) to confirm phase purity and scanning electron microscopy (SEM) to examine morphology. Electrochemical performance was evaluated through cyclic voltammetry (CV), galvanostatic charge-discharge (GCD), and electrochemical impedance spectroscopy (EIS) in an aqueous (NH₄)₂SO₄ electrolyte. The study investigated the redox behavior, charge storage mechanism, rate capability, and long-term cycling stability of LiMnO₂. The findings provide insights into the feasibility of ammonium-ion intercalation in LiMnO₂ and highlight the material's potential as a cathode for next-generation aqueous rechargeable batteries.

2 MATERIALS AND METHODS

The synthesis of LiMnO₂ via the solid-state reaction method was carried out through a multi-step process to ensure phase purity and homogeneity (Figure 2). High-purity MnCO₃ (≥99%) and LiOH·H₂O (≥98%) were first precisely weighed in a Li:Mn molar ratio of 1:1.05, with the slight lithium excess compensating for potential volatilization losses during hightemperature treatment. The precursors were thoroughly mixed and ground in an agate mortar and pestle for 30-60 minutes to achieve a uniform mixture. To enhance reactivity, the mixed powder underwent hydrothermal pre-treatment in a Teflon-lined autoclave at 120°C for 24 hours, promoting better precursor interaction. The resulting product was then calcined in a muffle furnace at 400°C for 12 hours (5°C/min heating rate) under static air to facilitate the solid-state reaction and crystallization of LiMnO₂. To remove impurities such as unreacted manganese oxides or lithium residues, the calcined material was stirred in 5 M HCl for 48 hours, followed by filtration and repeated washing with deionized water until neutral pH (~7) was achieved. The purified product was finally dried at 80°C for 12 hours to obtain the desired LiMnO₂ powder. For a purely solid-state approach without hydrothermal treatment, the mixture can alternatively be calcined at 600-800°C for 24 hours with intermediate grindings. This detailed procedure ensures the production of high-quality LiMnO₂ suitable for battery applications, with adjustments possible for targeting specific polymorphs like layered or orthorhombic structures.

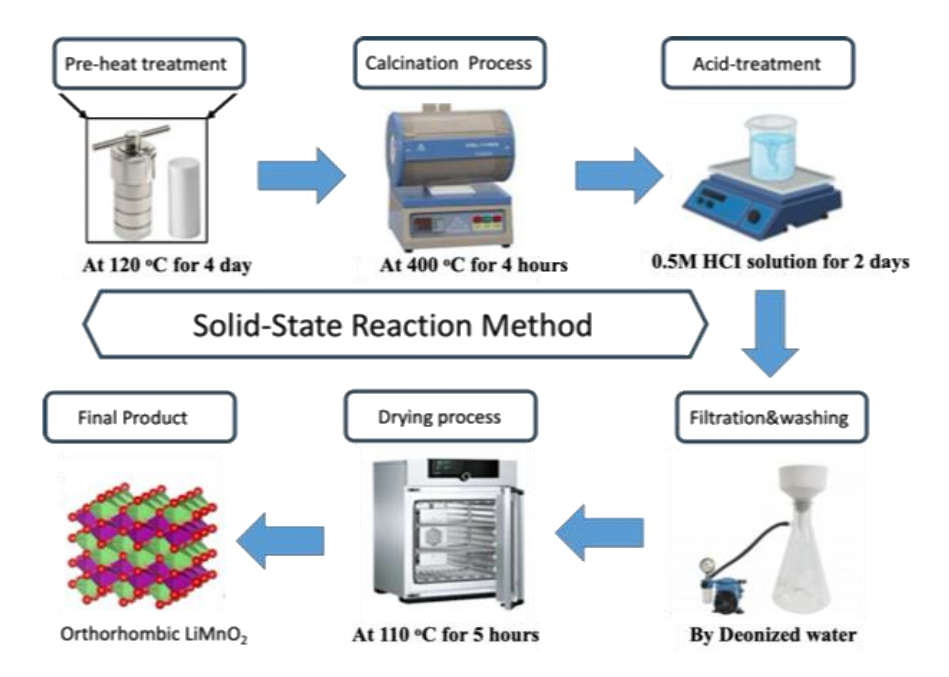


Figure 2. Schematic representation of the solid-state reaction synthesis process for LiMnO₂.

Following the synthesis of electroactive host materials (LiMnO₂), electrode slurries were separately prepared by homogenously mixing the active material, carbon black, and polyvinylidene fluoride (PVDF) in an 80:10:10 weight ratio. In this composition, carbon black functions as a conductive agent to enhance electron transport, while PVDF serves as a binder to improve electrode integrity and adhesion. The mixture was subsequently dispersed in N-methyl-2-pyrrolidone (NMP) as the solvent, ensuring uniform distribution of all components. The resulting slurry was continuously stirred on a magnetic stirrer overnight to achieve thorough homogenization, thereby optimizing the electrochemical performance and mechanical stability of the electrode. The electrode slurries were then cast using a doctor blade with a thickness of 1 mm onto a graphite plate, which served as the current collector. Subsequently, the coated electrodes were dried in an oven at 70°C to remove residual solvent and ensure proper adhesion of the active material to the current collector.

The battery configuration was assembled using a three-electrode glass beaker cell. The dried electrode slurries, previously cast onto graphite plates, were employed as the working electrode. A graphite rod was used as the auxiliary (counter) electrode to facilitate charge transfer, while an Ag/AgCl electrode served as the reference electrode to provide a stable reference potential. The electrodes were immersed in an aqueous electrolyte solution, ensuring proper ionic conductivity and electrochemical interaction. This setup enabled precise electrochemical measurements and characterization of the electrode materials.

The electrochemical performance of the LiMnO₂ cathode was investigated through several electrochemical techniques. Cyclic voltammetry (CV) tests were conducted in an aqueous (NH₄)₂SO₄ electrolyte within the voltage range of 0 V to 1.2 V vs. Ag/AgCl at room temperature. The CV was performed with a scan rate of 3 mV/s to assess the oxidation and reduction processes of the material. Each CV experiment was performed for 100 cycles to ensure reproducibility and assess electrochemical stability. Galvanostatic charge-discharge (GCD) tests were carried out within the same voltage window (0 V to 1.2 V vs. Ag/AgCl) using current densities ranging from 1C to 10C, where 1C corresponds to 148 mA/g, to evaluate the capacity, cycling stability, and rate performance of the cathode. Additionally, electrochemical impedance spectroscopy (EIS) was performed in the frequency range from 100,000 Hz to 0.1 Hz to analyze the charge transfer resistance and ion diffusion behavior with an applied AC amplitude of 10 mV. All electrochemical measurements were conducted using an Admiral Instrument Squid Stat Plus Potentiostat. In this study, the active mass loading was between 0.002 and 0.003 g, and the surface area of the active material was approximately 0.75 cm², ensuring consistency and reliability in the electrochemical evaluations.

The structural properties of the synthesized LiMnO₂ cathode were analyzed using X-ray diffraction (XRD). The crystal structure and phase purity of the synthesized LiMnO₂ were examined using X-ray diffraction (XRD) analysis. The measurements were conducted on a Bruker D8 Advance X-ray diffractometer equipped with a Cu K α radiation source (λ = 1.5406 Å), operating at 40 kV and 40 mA. The diffraction patterns were recorded in the 2 θ range of 10° – 80° with a step size of 0.02° and a scan speed of 1° /min.

3 RESULTS AND DISCUSSIONS

The XRD pattern of LiMnO₂, as shown in Figure 3a, reveals well-defined diffraction peaks, indicating a highly crystalline structure. The observed peaks correspond well with the standard JCPDS card 35-749 of orthorhombic LiMnO₂, confirming the successful phase formation without significant impurities. The most intense peak around $2\theta = \sim 40^{\circ}$ suggests a preferred orientation, which may be related to the synthesis conditions and the structural anisotropy of the material [20]. The absence of additional peaks from secondary phases, such as Mn₂O₃ or Mn₃O₄, indicates the phase purity of the synthesized sample [21]. Additionally, the sharpness of the peaks suggests a relatively large crystallite size and the peak broadening at lower angles may be attributed to micro-strain effects, which could impact the electrochemical properties of LiMnO₂ by influencing cation diffusion pathways [22]. The SEM images of

pristine LiMnO₂ synthesized via hydrothermal methods reveal a nanostructured, porous morphology with secondary agglomerates composed of fine primary particles (Figure 3b). The particle surfaces appear rough and loosely packed, with interconnected porous regions that are typical of hydrothermally synthesized oxides. This microstructure is advantageous for electrochemical applications, as it promotes electrolyte infiltration and shortens the ion charger diffusion paths. The particle sizes range from sub-micron to nanoscale, with no evidence of severe agglomeration or sintering. The uniform distribution and relatively homogeneous texture suggest controlled nucleation and growth during the hydrothermal process. Overall, the SEM analysis confirms that hydrothermal synthesis yields LiMnO₂ with a favorable porous architecture and nanoscale features, which could enhance the electrochemical kinetics and cycling stability in amonium-ion battery applications.

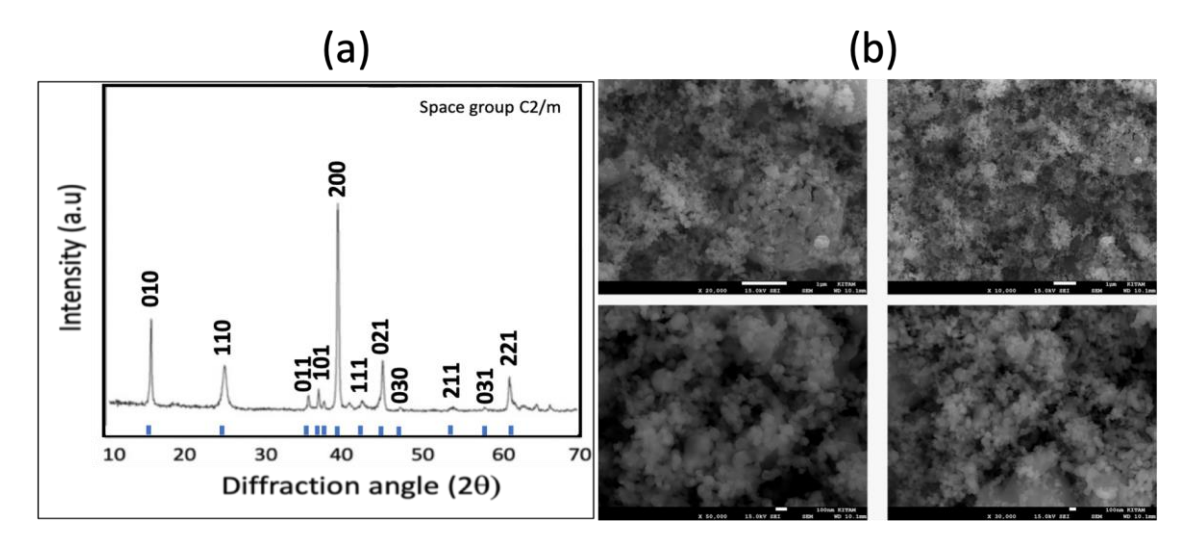


Figure 3. a) XRD pattern of orthorhombic LiMnO₂ showing well-defined diffraction peaks corresponding to the C2/m space group, confirming phase purity and crystallinity. b) SEM images of pristine LiMnO₂ synthesized via hydrothermal method.

The cyclic voltammetry (CV) curves of LiMnO₂ in 0.5 M (NH₄)₂SO₄ electrolyte exhibit two distinct electrochemical mechanisms. In Figure 4(a), which represents the electrochemical ion-exchange process, the oxidation peak appears at approximately 0.82 V vs. Ag/AgCl, while the reduction peak is observed at 0.41 V vs. Ag/AgCl. The interaction between ammonium ions and the host material following the Li-extraction process occurs through hydrogen bonding between the oxygen atoms of the host and the hydrogen atoms of the ammonium ions. This interaction is schematically illustrated in Figure 4c. The second cycle in Figure 4b exhibits an increase in current, suggesting structural activation and improved ion accessibility facilitated by NH₄⁺ insertion/extraction. This contrasts with the initial decline observed in Figure 4a (Li⁺-based process), highlighting the distinct redox kinetics of NH₄⁺ compared to Li⁺. The divergence

underscores the role of NH₄⁺ in enhancing electrochemical activity after the first cycle, possibly due to reduced kinetic barriers or optimized host structure rearrangement. The shape of the CV curve suggests a process influenced by ion diffusion and insertion, typically seen in battery-type materials [23, 24]. In Figure 4(b), corresponding to the NH₄⁺-based redox process, broader redox peaks are observed, indicating a more complex charge storage mechanism. The oxidation peaks occur at 0.89 V and 0.72 V vs. Ag/AgCl, while the reduction peaks appear at 0.53 V and 0.28 V vs. Ag/AgCl, suggesting multi-step redox transitions involving NH₄⁺ interactions with the electrode [25, 26]. The broader nature of the peaks and their relatively higher currents suggest a pseudocapacitive contribution, where NH₄⁺ ions participate not just in insertion/extraction but also in surface-controlled redox reactions [27]. The differences between Figures 4(a) and 4(b) highlight the dual role of NH₄⁺ in the system—acting as a charge carrier in an ion-exchange mechanism in Figure 4(a) and actively participating in redox reactions in Figure 4(b)—which significantly affects the electrochemical performance of the LiMnO₂ electrode in ammonium-based electrolytes.

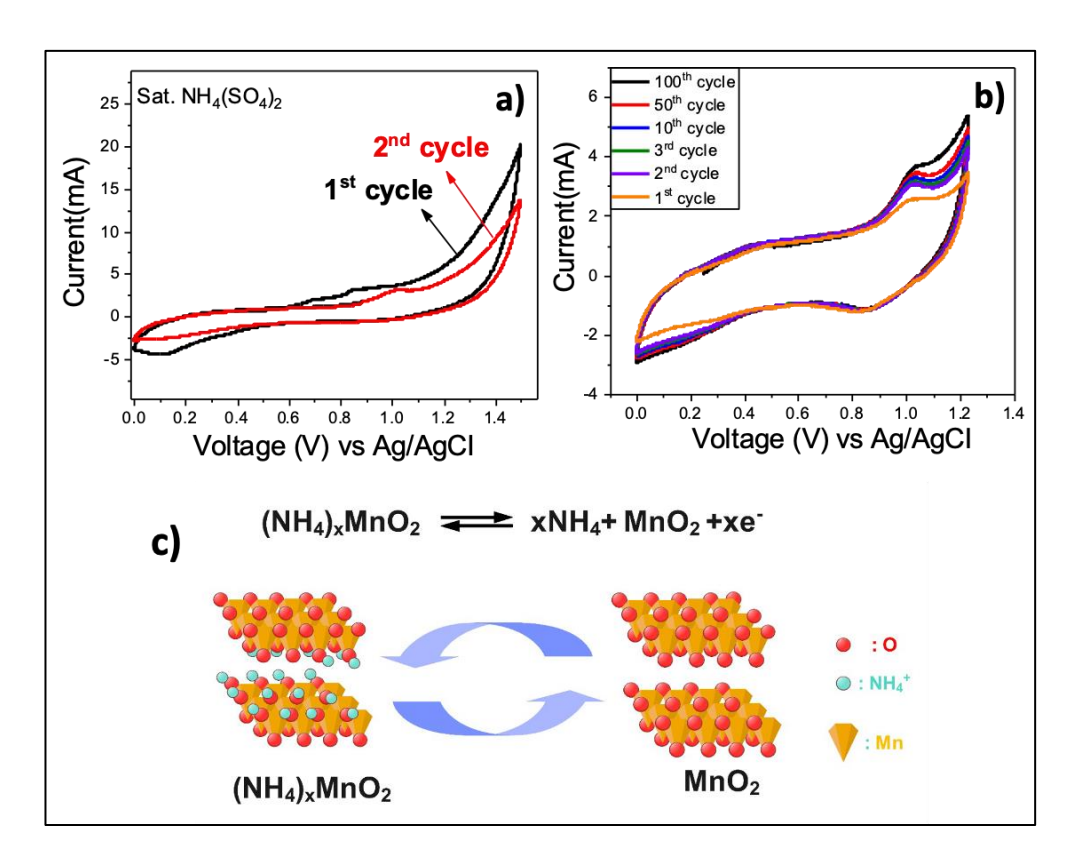


Figure 4. a) Electrochemical phase change from LiMnO₂ to (NH₄)_xMnO₂ by cyclic voltammetry analysis, and b) cyclic voltammogram of (NH₄)_xMnO₂ phase in saturated aqueous (NH₄)₂SO₄ electrolyte, and c) schematically representation of ammonium intercalation into the active host material.

The galvanostatic charge-discharge (GCD) curves at different C-rates (1C, 2C, 4C, 8C, and 10C) demonstrate the electrochemical performance of the electrode under varying current densities. At lower C-rates (1C and 2C), where 1C corresponds to a current rate that discharges the battery in one hour (for LiMnO₂, 1C is typically 148 mA/g, based on its theoretical capacity of approximately 148 mAh/g), the charge-discharge curves exhibit well-defined voltage plateaus, indicating efficient redox reactions and higher capacity due to slower ion diffusion and more complete electrochemical processes. However, as the C-rate increases to 4C, 8C, and 10C, the charge-discharge times shorten significantly, and the voltage plateaus become less distinct, suggesting increased polarization and kinetic limitations [28]. The observed capacity fading at higher C-rates indicates that the charge storage mechanism is affected by ion transport resistance, possibly due to NH₄+ diffusion barriers within the electrode structure. Despite this, if the electrode retains reasonable capacity at 10C, it implies good rate performance and fast charge transfer dynamics, making it suitable for high-power applications. The steep decline in capacity at higher C-rates suggests that further optimization, such as improving electrode conductivity or modifying the material structure, could enhance rate capability. Overall, the GCD analysis confirms that while the electrode material can sustain charge-discharge cycles over a wide range of C-rates, its electrochemical performance is limited by ion transport kinetics and internal resistance at higher current densities [29-31].

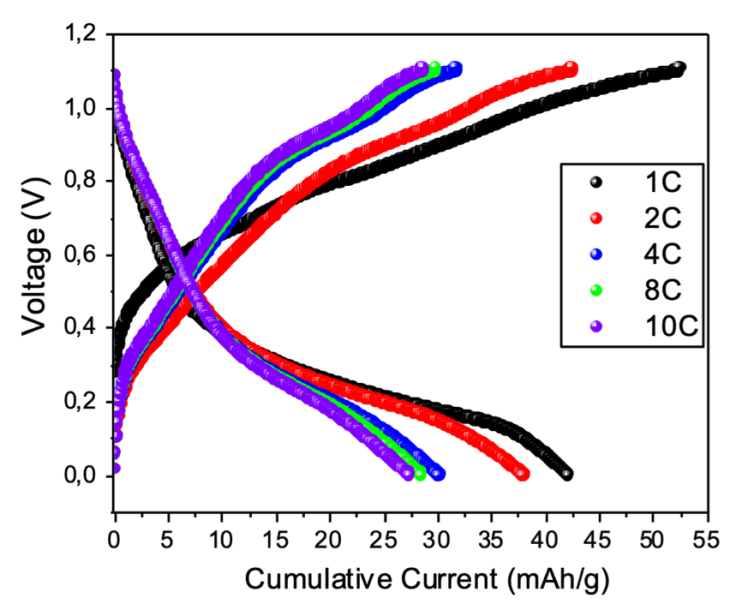


Figure 5. Electrochemical Performance of $(NH_4)_xMnO_2$ at different Current densities.

Figure 6a shows the discharge capacity of LiMnO₂ in a 2M (NH₄)₂SO₄ electrolyte at a 1C rate over 130 cycles. The electrode delivers an initial capacity of \sim 60 mAh/g, which drops slightly to \sim 50 mAh/g by the second cycle and then remains remarkably stable for the remaining

cycles, demonstrating excellent long-term cycling stability. This behavior suggests that the electrode undergoes minimal structural degradation or active material loss after the initial cycles. The mild acidic nature of (NH₄)₂SO₄ does not appear to cause significant Mn dissolution, unlike in stronger acidic environments. The stable capacity retention indicates that LiMnO₂ exhibits pseudocapacitive-like behavior, where surface-dominated charge storage mechanisms help maintain performance over extended cycling. The absence of severe capacity fade implies that the electrolyte-electrode interface remains relatively stable, possibly due to the formation of a passivating layer that prevents further side reactions. This makes LiMnO₂ in (NH₄)₂SO₄ a promising candidate for applications requiring long cycle life, though further optimization could improve the initial capacity loss. Figures 6b and 6c provide complementary electrochemical impedance spectroscopy (EIS) data, revealing interfacial and transport changes before and after cycling. The fresh electrode (Figure 6c) exhibits a small high-frequency semicircle, indicative of moderate charge-transfer resistance (R_{ct}), and a linear Warburg tail, reflecting efficient ion diffusion [15, 32, 33]. After cycling, the enlarged semicircle (Figure 6b) signals increased R_{ct} due to passivating SEI (solid electrolyte interphase) growth or Mn dissolution products, while the steeper Warburg slope suggests hindered Li⁺ diffusion from pore clogging or particle cracking. The zoomed-in Nyquist plot (Figure 6c) further highlights a rise in ohmic resistance (R_{Ω}) , likely from electrode delamination or electrolyte depletion. Together, these trends explain the capacity fade in Figure 6a: interfacial degradation exacerbates kinetic limitations, creating a feedback loop that accelerates performance loss.

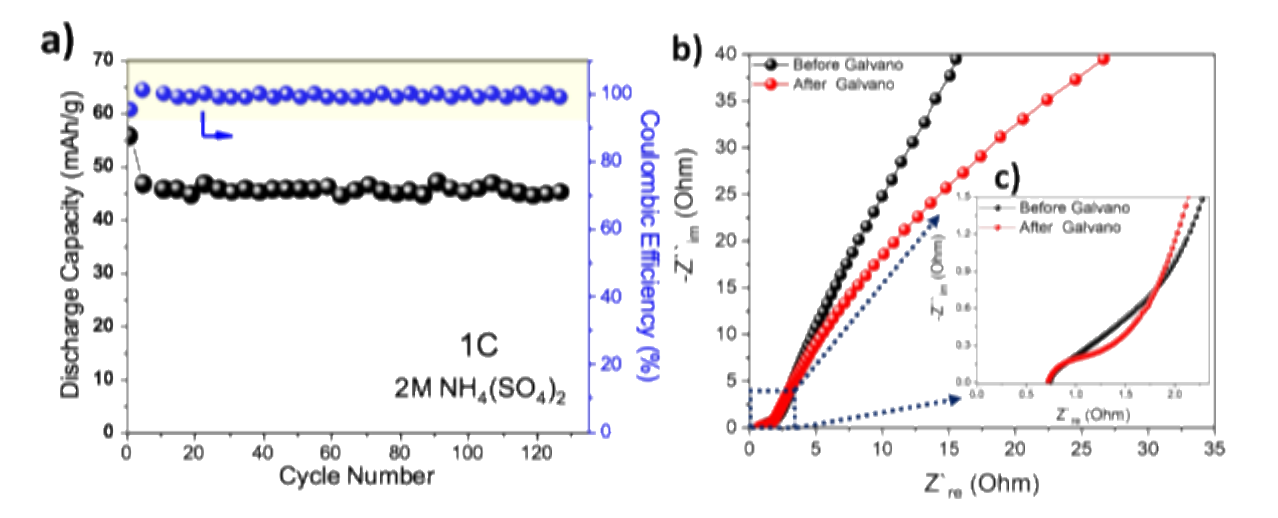


Figure 6. a) Discharge capacity (mAh/g) of LiMnO₂ in 2M (NH₄)₂SO₄ electrolyte at a 1C rate over 120 cycles. b) Nyquist plots of LiMnO₂ before and after galvanostatic charge-discharge testing, with c) showing a zoomed-in view of the high-frequency region.

The fitted equivalent circuit parameters from Figure 6b provide quantitative insights into the electrochemical behavior of the LiMnO2 system. The impedance spectra were fitted using a hierarchical equivalent circuit model accounting for all interfacial processes (Figure 7). This model intentionally separates the passive surface layer effects (R_{sh}||CPE_{sh}) from the electrode processes (Rct||CPE_t+W) to reflect their distinct physical origins – ionic transport through surface films versus Faradaic reactions at the electrode interface. The series resistance $(R_s = 4.8 \pm 0.2 \Omega)$, representing bulk electrolyte and contact resistances, was determined from the high-frequency real-axis intercept. A surface film branch ($R_{sh} = 15 \pm 2~\Omega \parallel CPE_{sh} = 5.2 \times 10^{-6}$ $F \cdot s^{n-1}$, $n = 0.92 \pm 0.03$) was included to model the high-frequency semicircle (10⁴-10² Hz), where R_{sh} quantifies ion conduction resistance through surface layers (e.g., SEI) and CPE_{sh} captures their capacitive properties, which differ fundamentally from the electrode's charge-transfer behavior. The dominant charge-transfer resistance ($R_{ct} = 135 \pm 5 \Omega$), derived from the midfrequency semicircle diameter (10²-10⁰ Hz), reflects the kinetic barrier for Faradaic reactions, while its associated double-layer CPE_t (1.2×10⁻⁵ F·sⁿ⁻¹,n= 0.88±0.02) accounts for electrode surface heterogeneity. The Warburg coefficient ($\sigma = 92 \pm 3 \ \Omega \cdot s^{-0.5}$), extracted from the lowfrequency linear slope (10°-10⁻² Hz), characterizes solid-state diffusion limitations. This circuit topology is specifically chosen because passive surface layers (e.g., native oxides) lack the Faradaic charge-transfer and diffusion elements required to describe active electrode processes. These parameters collectively demonstrate that while the interfacial charge transfer presents the dominant resistance, the system maintains reasonable ionic conductivity and surface properties for electrochemical processes. The relatively large R_{ct} value compared to R_s highlights that charge-transfer kinetics rather than ohmic losses constitute the primary limitation in this system [34, 35].

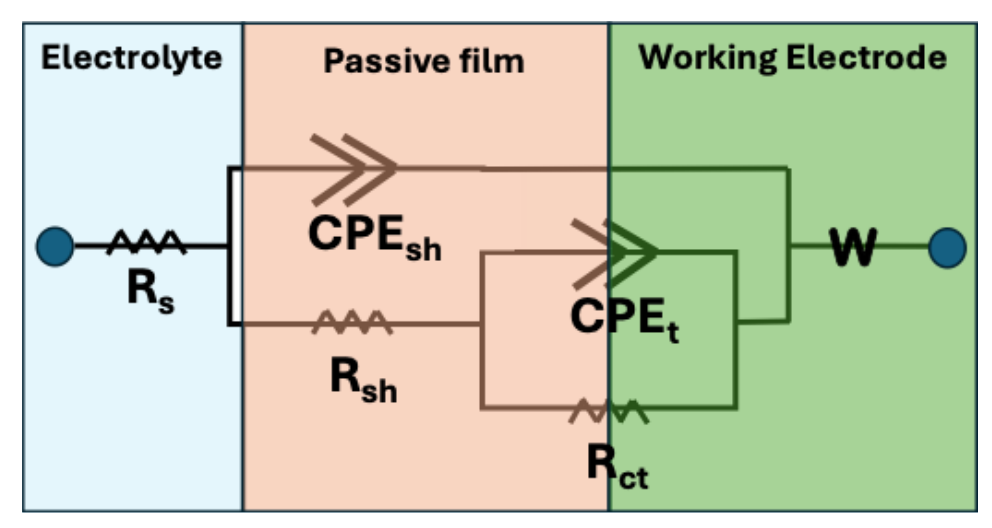


Figure 7. Equivalent Circuit for Nyquist plot of LiMnO₂ upon the Galvanostatic chargedischarge measurement at 2M (NH₄)₂SO₄ at 1C.

4 **CONCLUSION**

This study presents a comprehensive investigation of LiMnO₂ as a novel cathode material for ammonium-ion-based energy storage systems, marking its first application as a host electrode in this context. Structural and morphological characterization via XRD and SEM confirmed the successful synthesis of phase-pure, highly crystalline orthorhombic LiMnO₂ with a nanostructured, porous morphology composed of interconnected secondary agglomerates. The absence of secondary phases and sharp XRD diffraction peaks indicate high crystallinity, while the SEM analysis reveals a favorable porous architecture with rough, loosely packed particles ranging from sub-micron to nanoscale dimensions. This unique microstructure enhances electrolyte infiltration and shortens ion diffusion paths, contributing to improved electrochemical kinetics.

Electrochemical analyses provided valuable insights into the charge storage mechanisms and performance limitations of LiMnO₂ in (NH₄)₂SO₄ electrolyte. Cyclic voltammetry results revealed two distinct electrochemical behaviors: an ion-exchange process facilitating NH₄⁺ insertion/extraction and a redox-dominated process contributing to charge storage through surface-controlled reactions. The oxidation peaks at 0.89 V and 0.72 V vs. Ag/AgCl and reduction peaks at 0.53 V and 0.28 V vs. Ag/AgCl confirm the involvement of multi-step redox transitions. The galvanostatic charge-discharge tests demonstrated that the electrode delivers an initial discharge capacity of ~60 mAh/g at a 1C rate, and experiences high-capacity retention over 130 cycles. At higher C-rates (4C, 8C, and 10C), the voltage plateaus become less distinct due to increased polarization and kinetic limitations, with a notable capacity decline.

Long-term cycling performance in 2M (NH₄)₂SO₄ electrolyte demonstrated excellent stability, with the discharge capacity stabilizing at ~50 mAh/g after the second cycle and maintaining this value over 130 cycles. This remarkable capacity retention suggests minimal structural degradation and effective suppression of Mn dissolution in the mildly acidic electrolyte environment. Electrochemical impedance spectroscopy showed only a moderate increase in charge transfer resistance (Rct) from 135 Ω to ~200 Ω after prolonged cycling, indicating relatively stable interfacial kinetics. The fitted equivalent circuit analysis revealed that while some interfacial changes occurred during cycling, the system maintained favorable charge-transfer characteristics that supported the observed long-term stability. These findings highlight the robust electrochemical behavior of LiMnO₂ in (NH₄)₂SO₄ electrolyte, with the

stable capacity retention suggesting dominant pseudocapacitive charge storage mechanisms that are less susceptible to the structural degradation typically observed in bulk intercalation processes.

The results demonstrate that LiMnO₂ effectively functions as a stable host material for ammonium-ion storage, exhibiting remarkable cycling stability with a retained capacity of ~50 mAh/g over 130 cycles in (NH₄)₂SO₄ electrolyte. This performance, coupled with its pseudocapacitive charge storage behavior, positions LiMnO₂ as a promising cathode candidate for next-generation ammonium-ion batteries. The minimal capacity fade and moderate interfacial resistance growth confirm its structural resilience against Mn dissolution and phase degradation in mildly acidic electrolytes—a critical advantage for sustainable energy storage systems. To further advance this technology, future research should focus on optimizing LiMnO₂'s host properties through nanostructuring or composite design to enhance NH₄⁺ diffusion kinetics while maintaining its inherent stability. Additionally, exploring concentrated or hybrid electrolytes could unlock higher capacities without compromising cyclability. This work establishes LiMnO₂ as a viable host framework for ammonium-ion batteries and provides a foundation for developing high-performance, low-cost energy storage alternatives to lithium-based systems.

Acknowledgements

The authors gratefully acknowledge the financial support provided by Ondokuz Mayıs University Scientific Research Projects Coordination Unit (OMU BAP) under project number [Project no: 5202]. This support was instrumental in conducting the research and acquiring the necessary materials and equipment.

Conflict of Interest Statement

There is no conflict of interest between the authors.

Statement of Research and Publication Ethics

The study is complied with research and publication ethics.

Artificial Intelligence (AI) Contribution Statement

This manuscript was entirely written, edited, analyzed, and prepared without the assistance of any artificial intelligence (AI) tools. All content, including text, data analysis, and figures, was solely generated by the authors.

Contributions of the Authors

Burak Tekin, as the corresponding author, led the study's conception and design, performed electrochemical measurements, created the graphs, interpreted the results, and wrote and edited the manuscript. Melisa Ucan and Dilara Ozgenc conducted the material characterization and contributed to the electrochemical testing.

REFERENCES

- [1] M. D. Ahmed and K. M. Maraz, "Revolutionizing energy storage: Overcoming challenges and unleashing the potential of next generation Lithium-ion battery technology," *Materials Engineering Research*, vol. 5, no. 1, pp. 265-278, 2023.
- [2] A. Kulkarni, C. Padwal, J. MacLeod, P. Sonar, T. Kim, and D. Dubal, "Toward Safe and Reliable Aqueous Ammonium Ion Energy Storage Systems," *Advanced Energy Materials*, vol. 14, no. 31, p. 2400702, 2024.
- [3] R. Demir-Cakan, M. R. Palacin, and L. Croguennec, "Rechargeable aqueous electrolyte batteries: from univalent to multivalent cation chemistry," *Journal of Materials Chemistry A*, vol. 7, no. 36, pp. 20519-20539, 2019.
- [4] B. Tekin, "Nafion-protected Na3V2 (PO4) 3 electrodes for aqueous zinc-ion batteries: A breakthrough in dissolution resistance and electrochemical enhancement," *Materials Science and Engineering: B*, vol. 307, p. 117534, 2024.
- [5] B. Tekin, S. Sevinc, M. Morcrette, and R. Demir-Cakan, "A new sodium-based aqueous rechargeable battery system: the special case of Na0. 44MnO2/dissolved sodium polysulfide," *Energy Technology*, vol. 5, no. 12, pp. 2182-2188, 2017.
- [6] J. Huang, Z. Guo, Y. Ma, D. Bin, Y. Wang, and Y. Xia, "Recent progress of rechargeable batteries using mild aqueous electrolytes," *Small Methods*, vol. 3, no. 1, p. 1800272, 2019.
- [7] X. Wu, Y. Qi, J. J. Hong, Z. Li, A. S. Hernandez, and X. Ji, "Rocking-chair ammonium-ion battery: a highly reversible aqueous energy storage system," *Angewandte Chemie International Edition*, vol. 56, no. 42, pp. 13026-13030, 2017.
- [8] Y. Yao *et al.*, "Electrochemical synthesis of ammonia from nitrogen under mild conditions: current status and challenges," *Electrochemical Energy Reviews*, vol. 3, pp. 239-270, 2020.
- [9] D. Chao *et al.*, "Roadmap for advanced aqueous batteries: From design of materials to applications," *Science advances*, vol. 6, no. 21, p. eaba4098, 2020.
- [10] S. Dong *et al.*, "Ultra-fast NH4+ storage: strong H bonding between NH4+ and bi-layered V2O5," *Chem*, vol. 5, no. 6, pp. 1537-1551, 2019.
- [11] C. Li *et al.*, "Achieving a high-performance Prussian blue analogue cathode with an ultra-stable redox reaction for ammonium ion storage," *Nanoscale Horizons*, vol. 4, no. 4, pp. 991-998, 2019.
- [12] Y. Zhang *et al.*, "A novel aqueous ammonium dual-ion battery based on organic polymers," *Journal of Materials Chemistry A*, vol. 7, no. 18, pp. 11314-11320, 2019.
- [13] X. Wu *et al.*, "NH4+ topotactic insertion in berlin green: an exceptionally long-cycling cathode in aqueous ammonium-ion batteries," *ACS Applied Energy Materials*, vol. 1, no. 7, pp. 3077-3083, 2018.
- [14] W. Zheng *et al.*, "Advanced ammonium salt materials for electrochemical energy storage: Recent progress and future perspectives," *Chemical Engineering Journal*, vol. 454, p. 140194, 2023.
- [15] Y. Sun *et al.*, "Ammonium-ion energy storage devices for real-life deployment: storage mechanism, electrode design and system integration," *Energy & Environmental Science*, vol. 16, no. 12, pp. 5568-5604, 2023.
- [16] R. Yuan, H. Jiao, H. Zhu, D. Fang, and S. Jiao, "In situ characterization techniques and methodologies for high-temperature electrochemistry," *Chem,* vol. 9, no. 9, pp. 2481-2508, 2023.

- [17] G. N. P. F. Franklin, "Operando studies by SECM, ECD, and EQCM of materials for electrochemical energy storage," Université Paul Sabatier-Toulouse III, 2023.
- [18] G. Gourdin and V. Doan-Nguyen, "In situ, operando characterization of materials for electrochemical devices," *Cell Reports Physical Science*, vol. 2, no. 12, 2021.
- [19] Z. Zhao *et al.*, "A 2.75 V ammonium-based dual-ion battery," *Angewandte Chemie International Edition*, vol. 61, no. 51, p. e202212941, 2022.
- [20] X. Tu and K. Shu, "X-ray diffraction study on phase transition of orthorhombic LiMnO2 in electrochemical conversions," *Journal of Solid State Electrochemistry*, vol. 12, no. 3, pp. 245-249, 2008.
- [21] S.-h. Wu and M.-t. Yu, "Preparation and characterization of o-LiMnO2 cathode materials," *Journal of Power Sources*, vol. 165, no. 2, pp. 660-665, 2007.
- [22] M. A. Kebede, "An investigation of the lattice parameter and micro-strain behaviour of LiMn2O4 coated with LiMn1. 5Ni0. 5O4 to attain high-rate capability and cycling stability," *Journal of Energy Storage*, vol. 72, p. 108602, 2023.
- [23] C. Costentin, "Cyclic voltammetry to study dynamics of ion insertion in porous materials," *Advanced Energy and Sustainability Research*, vol. 5, no. 5, p. 2300242, 2024.
- [24] J. Heinze, "Cyclic voltammetry—"electrochemical spectroscopy". New analytical methods (25)," *Angewandte Chemie International Edition in English*, vol. 23, no. 11, pp. 831-847, 1984.
- [25] F. Marken, A. Neudeck, and A. M. Bond, "Cyclic voltammetry," *Electroanalytical methods: guide to experiments and applications*, pp. 57-106, 2010.
- [26] P. T. Kissinger and W. R. Heineman, "Cyclic voltammetry," *Journal of chemical education*, vol. 60, no. 9, p. 702, 1983.
- [27] W. Pholauyphon, P. Charoen-Amornkitt, T. Suzuki, and S. Tsushima, "Perspectives on accurately analyzing cyclic voltammograms for surface-and diffusion-controlled contributions," *Electrochemistry Communications*, vol. 159, p. 107654, 2024.
- [28] X. Zhang *et al.*, "Unlocking High-Performance Ammonium-Ion Batteries: Activation of In-Layer Channels for Enhanced Ion Storage and Migration," *Advanced Materials*, vol. 35, no. 40, p. 2304209, 2023.
- [29] W. F. Wu *et al.*, "A High-Rate and Ultrastable Ammonium Ion-Air Battery Enabled by the Synergy of ORR and NH4+ Storage," *Advanced Materials*, p. 2415476.
- [30] G. Yüksek and A. Alkaya, "Effect of the Depth of Discharge and C-Rate on Battery Degradation and Cycle Life," in 2023 14th International Conference on Electrical and Electronics Engineering (ELECO), 2023: IEEE, pp. 1-5.
- [31] R. Zheng *et al.*, "Ammonium ion batteries: material, electrochemistry and strategy," *Angewandte Chemie*, vol. 135, no. 23, p. e202301629, 2023.
- [32] H. J. Watson and M. N. Frolick, "Determining information requirements for an EIS," *MIS quarterly,* pp. 255-269, 1993.
- [33] Z. Bao *et al.*, "An acetate electrolyte for enhanced pseudocapacity capacity in aqueous ammonium ion batteries," *Nature Communications*, vol. 15, no. 1, p. 1934, 2024.
- [34] J. Wu, "Understanding the electric double-layer structure, capacitance, and charging dynamics," *Chemical Reviews*, vol. 122, no. 12, pp. 10821-10859, 2022.
- [35] D. M. Adams *et al.*, "Charge transfer on the nanoscale: current status," *The Journal of Physical Chemistry B*, vol. 107, no. 28, pp. 6668-6697, 2003.